Gas phase trapped ion studies of collisionally formed MgC_{60}^+ complexes

R. I. Thompson,[a] M. Welling,[b] H. A. Schuessler,[c] and H. Walther
Max-Planck-Institut für Quantenoptik, Hans-Kopfermann-Str. 1, D-85748 Garching bei München, Germany

(Received 8 January 2002; accepted 26 March 2002)

A series of experiments were performed to study the formation of MgC_{60}^+ complexes via $Mg^+ + C_{60}$ collisions, and to study the structure and stability of the resulting complexes via optical spectroscopy and mass spectrometry. Collision experiments were carried out in a linear ion trap apparatus under conditions of controlled collision energies, reactant densities, and buffer gas pressure. Ion trap mass spectrometry was used to measure the relative reaction rates for complex formation, charge transfer, and fragmentation reactions in $Mg^+ + C_{60}$ collisions. Laser-induced photodissociation was then used to study the MgC_{60}^+ complexes in order to measure their stability and identify their molecular structure. Absolute photodissociation cross sections were determined for complexes generated at low collision energies and reactant densities over the wavelength range of 1300–280 nm and were in the range from 2×10^{-20} cm^2 to 5×10^{-17} cm^2 in magnitude. The shape of the generated cross-section curve indicates that at low collision energies most of these complexes are exohedrals. More refined measurements of samples generated at optimum buffer gas pressures and higher collision energies demonstrated the existence of a second more slowly dissociating fraction that apparently results from the presence of endohedral complexes. © *2002 American Institute of Physics.* [DOI: 10.1063/1.1478698]

I. INTRODUCTION

The study of metallofullerenes in condensed phases is an active and wide-ranging field, both in its history and in the breadth of complexes that have been studied. Unfortunately, one of the drawbacks of this field is its inability to look at samples in the limit of an isolated molecule either during the generation of the complex, or afterwards. In addition, it is very difficult to tightly control the experimental conditions such as reaction energy and reactant densities during the generation process. Instead it is necessary to look at bulk properties and to control the bulk parameters while studying the complexes in the solid, powder, or solution phases (e.g., Refs. 1, 2). Gas phase work on fullerenes and fullerene complexes has been limited to mass spectrometric (e.g., Refs. 3–5) and short pulse photoionization studies (e.g., Ref. 6) of molecular beams. As a complementary alternative to these techniques for this field of study, we present a novel technique for both generating and studying ionic metallofullerene complexes in the gas phase, if needed down to the single molecule level. A linear ion trap is used to serve as an environment for collisions between neutral C_{60} molecules and charged Mg^+ ions. The collision energy, ranging from near 0 to 200 eV, particle densities, and reaction times are all controlled, while the charged product molecules are stored in the ion trap. Once formed, the complexes are cooled and stabilized through buffer gas collisions. Lasers are used to probe the stability of the complexes formed under different experimental conditions and to determine their molecular structure. Although some experiments have been carried out studying relatively short-lived complexes, the technique presented here observes the complexes over relatively long time periods (in excess of minutes), allowing the determination of the long term stability of the complexes in their low vibrational states.

II. EXPERIMENTAL APPARATUS AND TECHNIQUES

The experimental apparatus and techniques are extensively described in a separate publication.[7] Therefore, only a brief outline of the apparatus and techniques will be provided here.

The linear-geometry, radio frequency (RF) ion trap used in these experiments has a design based on a modified RF quadrupole mass spectrometer electrode arrangement. Four symmetrically positioned cylindrical electrodes are used to generate a RF trapping field, which holds the ions in the *X* and *Y* directions. The electrodes are divided into three electrically-isolated segments that carry identical RF fields, but independent dc fields (see Fig. 1). These dc fields, combined with those generated by on-axis end-cap electrodes are used to control the motion along the *Z*-axis of the trap, either to hold or accelerate the ions. The RF trapping parameters are mass dependent, allowing the trap itself to act as a mass spectrometer. The main detection technique utilizes a second RF field to parametrically excite the secular motion of the ions within the trap. The frequency of oscillation of an ion is mass dependent, and when a quadrupole electric field is applied at twice the frequency of the ion's motion, ions with the selected mass have the amplitude of their motion excited parametrically. For a strong enough field, the ions are driven

[a]Author to whom correspondence should be addressed. Permanent address: Department of Physics and Astronomy, University of Calgary, 2500 University Drive NW, Calgary, Alberta T2N 1N4, Canada. Electronic mail: thompson@phas.ucalgary.ca
[b]Present address: MTU, DiamlerChrysler, Munich, Germany.
[c]Permanent address: Department of Physics, Texas A&M University, College Station, Texas 77843-4242.

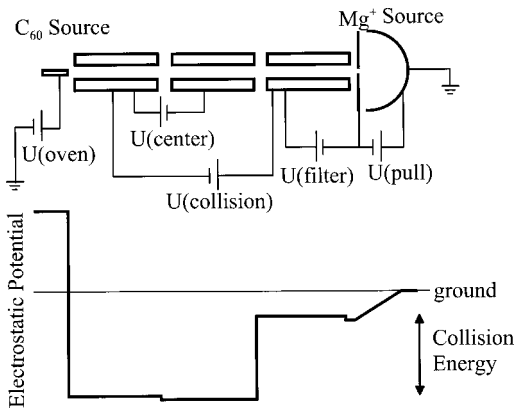

FIG. 1. Schematic top-view diagram of the ion trap electrodes and dc electric field potentials demonstrating ion trap operation in the ion–molecule collision mode.

out of the trap and collected by a biased electron multiplier tube (EMT, see Fig. 2). Scanning the excitation field generates a mass spectrum with an $m/\Delta m$ resolution of between 200 and 800 amu, depending on the mass range being examined. A second technique, referred to as *q*-scanning, simply reduces the trapping field strength until the trap depth felt by the selected mass is so low that the ion can be pulled out of the trap by the bias field of the external EMT. This technique has a much lower resolution than secular excitation, but covers rather large mass or charge ranges quickly, and has a high detection sensitivity.

The fullerene complexes are generated as follows. A small molecular oven, filled with powdered C_{60}, is positioned outside one end of the trap, on the trap axis. The oven is heated to generate a diffuse beam of neutral C_{60} molecules impinging into the trap (Fig. 2). At the opposite end, a second atomic oven is filled with solid magnesium, and when heated, the diffuse Mg beam is ionized by electron bombardment to form Mg^+ ions, which are then injected into the ion trap. A special focusing field, generated by a curved electrode, is used to inject the ions through an aperture and into the trap along the trap axis. The segmenting of the trap allows the C_{60} end to be maintained at a lower dc potential than the Mg^+ end of the trap (Fig. 1). Thus the Mg^+ ions are accelerated by a step potential before they interact with the C_{60} beam. Controlling the step potential size controls the collision energy. The spread in the kinetic energy of the Mg^+ ions is determined by the spread in the ion energies coming

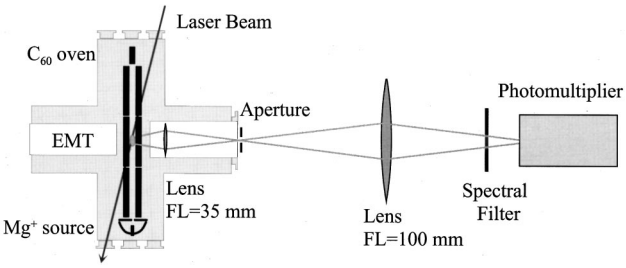

FIG. 2. Schematic diagram of the optical arrangements used for fluorescence probing of the trapped ions. EMT indicates the electron multiplier tube used for charged particle detection during ion trap mass spectrometry.

out of the ion source, which, within limits, can be controlled by a filter potential generated between the ion source and the input of the ion trap. Under normal operating conditions, this full-width half-maximum energy spread is approximately 3 eV. A computer system is used to control the ion formation, complex generation, and trap loading process, as well as the laser exposure (see next paragraph) and mass spectrometric analysis stages.

Laser spectroscopy is generally used as part of the analysis of the product ions. The probe laser passes through the sample volume at an angle of 15° with respect to the trap axis, which is necessary since the atomic and molecular ovens are positioned along the axis (Fig. 2). A series of different cw laser sources, including diode, helium–neon, ring dye, and doubled dye lasers, are used to provide radiation in the near infrared, visible, and ultraviolet regions of the optical spectrum. Once the trap is loaded with a sample, computer-controlled apertures are used to expose the sample to laser radiation for adjustable time periods. During the exposure, an optical imaging system is used to collect radiation scattered at right angles to the trap axis and focus the radiation onto the cathode of a cooled photomultiplier tube (PMT). This signal, together with the probe laser intensity recorded by a photodiode, are stored in the computer during laser exposure. After exposure, a high-resolution parametric mass scan is used to empty the trap while determining the resulting molecular composition of the trapped ion cloud. The computer system is designed to repeatable load practically identical samples into the trap for probing with different intensities, exposure times, or wavelengths of laser radiation.

III. RESULTS AND DISCUSSION

The results of this work fall into the two general categories, namely, collision reaction data and laser photodissociation spectra. The former investigates the physics of the formation of the complexes and subsidiary fullerene fragmentation processes, while the latter measures the complexes' stability and different dissociation paths leading to its destruction. Although very different types of measurements, these results complement each other well to form a comprehensive picture of the reaction dynamics and the structure of the complexes. We will first discuss the collision data and then the laser irradiation results.

A. Collisional reactions of C_{60} with Mg^+

C_{60} molecules and Mg^+ ions are injected at opposite ends of the linear ion trap arrangement, a dc step potential 1/3 of the way along the trap is then used to vary the collision energy of the Mg^+ ions before they collide with the C_{60} molecules. After the collision, it is imperative that the vibrational motion of the collisionally generated complex is quickly dissipated. This is effected by viscous drag cooling in a helium buffer gas at about 10^{-6} Torr. Such collisions stabilize the complexes by quenching their vibrational excitations. The complexes are stored in the trap until they are analyzed using parametric secular excitation for ion trap mass spectrometry. Oven temperature, buffer gas pressures, and step and filter potential voltages are used to control such

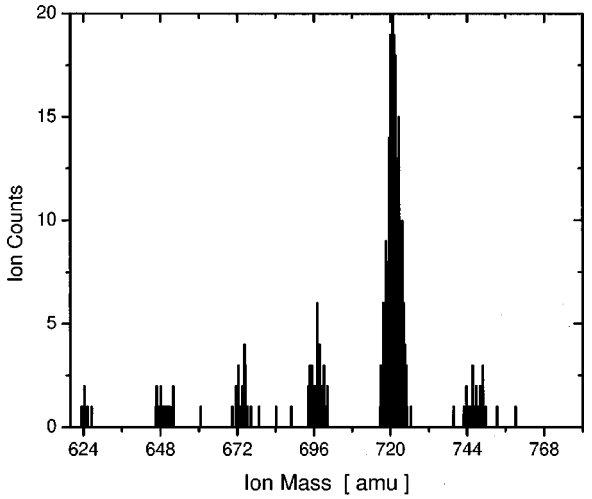

FIG. 3. Typical mass spectrum of the products from a $Mg^+ + C_{60}$ energy resolved collision experiment carried out with an ion acceleration potential of 60 eV. The peaks at 624, 648, 672, and 696 amu are fullerene fragment ions, while the peaks at 720 and 744 amu are C_{60}^+ and MgC_{60}^+ complexes, respectively.

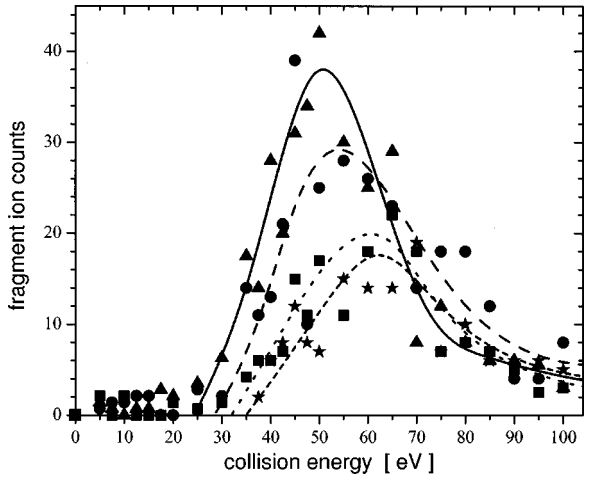

FIG. 4. Mass-resolved determination of the generation of fullerene fragment ions by Mg^+ bombardment of C_{60} as a function of the ion acceleration potential. The correspondence between fragment identity and symbol is C_{58}^+ (▲), C_{56}^+ (●), C_{54}^+ (■), and C_{52}^+ (★).

experimental parameters as reactant density, buffer gas collision rates, and Mg^+ kinetic energy during the collision processes.

In order to maximize the kinetic energy selectivity, and minimize fullerene destruction through excessive multiple collisions with Mg^+ ions, the trap potential in the collision studies is amplitude-modulated. The modulation amplitude is selected such that the motion of the massive fullerene and fullerene-complex ions is always stable, but the Mg^+ ions are stable only for approximately 1/3 of the time. This allows the Mg^+ ions to leak out of the trap before they lose significant collision energy through buffer gas collisions, and before too many of them collect in the trap. The trapping field modulation results in relatively slow reaction rates, but was implemented to obtain energy resolved data. In the photodissociation experiments discussed in Sec. III B, ion yield was the main criterion. Therefore, for these measurements the trap potential was not modulated.

Each collision experiment results in mass spectra of the form shown in Fig. 3. The collection efficiency with this form of mass spectrometry is less than 1% so the number of ions detected is only proportional to the number of ions stored in the trap. At a mass of 744 amu there appears a peak corresponding to MgC_{60}^+ complexes formed by the attachment of a Mg^+ ion to a C_{60} fullerene molecule. Next to this peak at mass 720 amu is the C_{60}^+ peak, which results from charge transfer of one electron pulled from a C_{60} molecule by a Mg^+ ion. Finally, at the masses 696, 672, 648, etc. amu one sees the presence of the fullerene fragments caused by the breaking off of C_2 units from the fullerene molecule by collisions with fast Mg^+ ions.

1. Fragmentation

Considering first the fragmentation reaction, Fig. 4 shows the data collected at different collision energies for the generation of the first 4 fullerene fragment ions. The main cause of the scatter in the data lies in the small number of collision processes due to the slow rate of these reactions caused by the weak energy-selected ion beam. The most obvious result is that fragmentation does not happen at low collision energies. Due to the high stability of the C_{60} cage, significant energy is required to knock off a C_2 fragment with significant fragmentation only occurring above 25 eV. However, note that once fragmentation from C_{60} to C_{58} begins to occur further steps down to C_{56}, C_{54}, and so on, follow with relatively small amounts of additional energy (a few eV) being required. This is consistent with the well-established result that C_{60} dissociates by sequential loss of C_2 fragments rather than removal of larger carbon pieces such as C_4 or C_6.[8] By plotting all of the data together, it can clearly be seen that all of the fullerene fragment curves roughly mirror each other as a function of a collision energy.

The exact mechanism of the fragmentation reaction of C_{60} to C_{58}^+ is not completely clear. It could occur in the single step of

$$C_{60} + Mg^+ \rightarrow C_{58}^+ + C_2 + Mg, \tag{A}$$

or it could proceed in multiple step processes involving a separate charge transfer process such as

$$C_{60} + Mg^+ \rightarrow C_{60}^{+*} + Mg, \tag{B}$$

$$C_{60}^{+*} \rightarrow C_{58}^+ + C_2^*, \tag{C}$$

or

$$C_{60} + Mg^+ \rightarrow C_{60}^+ + Mg, \tag{D}$$

$$C_{60}^+ + X \rightarrow C_{58}^+ + C_2 + X, \tag{E}$$

where X is a high-energy charged or neutral atom, molecule or fragment. The similar shapes of the fragmentation curves and the charge transfer curve (Fig. 5) suggest that at least some of the fragmentation may be following the latter route, reaction (D) followed by reaction (E).

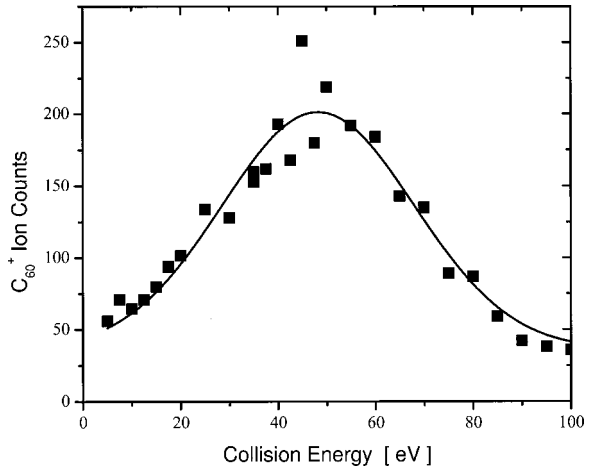

FIG. 5. Mass-resolved observations of C_{60}^+ ions generated by charge transfer from C_{60} to Mg^+ as a function of the ion acceleration potential. The solid line is a Gaussian fit to the data.

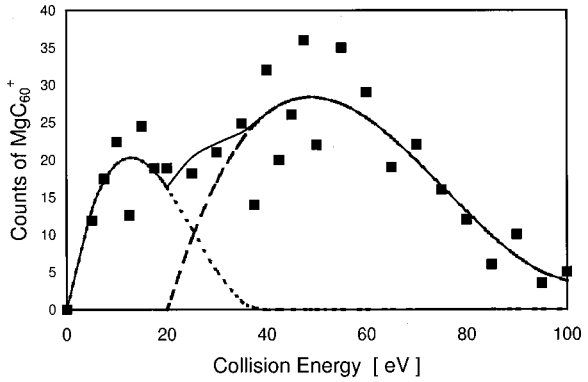

FIG. 6. Mass-resolved observations of the formation of MgC_{60}^+ complexes via $Mg^+ + C_{60}$ collisions as a function of the ion acceleration potential. The dashed line is a third-order polynomial fit to the high energy data ($E \geqslant 30$ eV). The dotted line is a third-order polynomial fit to the low energy data (see text). The narrow solid line is the sum of the two fits.

2. Charge transfer

Figure 5 shows the dependence of the yield of the charge transfer reaction on the collision energy. The number statistics for this measurement are much better than those for either the fragmentation or complex formation reactions, indicating that under these conditions charge transfer is a dominant reaction. The curvature displayed by these data appears to have a definite although broad resonance nature to it. The Gaussian fit to the data yields a peak energy of 48.2 ± 1.0 eV, and a peak width of 40 ± 4 eV. This feature can be explained by the Massey Criterion for near resonance charge transfer.[9] The Mg and C_{60} ionization potentials are very similar (7.644 and 7.57 ± 0.01 eV, respectively[10,11]). Thus the energy difference between the state $Mg^+ + C_{60}$ and the state $Mg + C_{60}^+$ is merely 0.074 ± 0.01 eV, corresponding to a frequency difference of 18 THz. In a semiclassical model, a charged particle passing the fullerene molecule in a straight-line trajectory generates an electric pulse and the Fourier transform of the electric pulse generated by a 50 eV Mg^+ ion passing the fullerene molecule peaks at approximately 20 THz, resonantly inducing the charge transfer.

More quantitatively, the first order transition probability for a Massey Criterion transition is given by

$$P_{o\to f}^1 = |C_{of}^1(\infty)|^2, \tag{1}$$

where

$$C_{of}^1(\infty) = \frac{1}{i\hbar v}\int_{-\infty}^{\infty} V_{fo}(r) e^{i\omega_{fo} z/v} dz, \tag{2}$$

and v = ion velocity, $V_{fo}(r)$ = interaction potential, ω_{fo} = transition frequency, $r^2 = b^2 + z^2$.

In general, Eq. (2) can be optimized either analytically or numerically for any given interaction potential to determine the velocity that results in the maximum transition probability. This velocity can be expressed in the form,

$$v_{\text{opt}} = k\omega_{fo}\rho, \tag{3}$$

where ρ is the interaction length of the potential and k is a constant of proportionality dependent only on the shape of the interaction. Using this approach it is possible to show that the peak demonstrated in Fig. 5 is a Massey-type transition for the interaction of a Mg^+ ion and a C_{60} molecule, assuming that the interaction potential is of short range and does not extend beyond the electron cloud. In fact, the fit is best to an analytical function is for a square-barrier potential that has a range of about 7 Å, which is within the cloud of electrons but outside the fullerene cage.

Further confirmation of the occurrence of Massey-type charge exchange in Mg^+ collisions is the lack of a charge exchange resonance peak in the equivalent measurement of collisions between Ne^+ ions and C_{60}. Such a study was carried out by another group[12] and separately by ourselves, with no resonance peak being observed. Due to the much higher ionization potential of Ne, the Massey criterion peak should be shifted into the keV range, and is therefore not observable in our $Ne^+ + C_{60}$ collision studies carried out below 100 eV.

3. Complex formation

Figure 6 shows the rate of complex generation as a function of collision energy. All of the data points were taken with the method just described, except for the one close to 0 eV. This point was observed by loading the trap with Mg^+ ions and collisionally cooling them to near room temperature before turning on the C_{60} oven. No fragment ions or complexes were detected, although some C_{60}^+ formed by charge exchange was observed (Fig. 6). This suggests that there is a small activation barrier to the formation of any complexes, endohedral or exohedral, in the reaction $Mg^+ + C_{60}$. This differs drastically from the formation of other fullerene complexes such as MnC_{60}^+, where the formation of exohedral complexes has no activation barrier and in fact is peaked at 0 eV.[13]

The shape of the curve that the data follow in Fig. 6 displays two partially resolved peaks, as indicated by the polynomial fitting curves. The data were fit in two steps. First, the 30–100 eV data were fit to a third order polynomial (dashed line). The results of this fit was subtracted from the raw data and the result was fit to a second third-order polynomial for the data between 0 and 37.5 eV (dotted line). In

each of the two fits, the value was fixed to zero outside the listed range of powers. The sum of the two fits yields the solid curve, which is a good match to the observed data, but demonstrates poor resolution of the two peaks.

Based on similar results with other guest atoms such as Mn^+ (Ref. 13) it is not unreasonable to expect two peaks, with a lower energy exohedral peak and a higher energy endohedral peak. For Mn^+ the two peaks are resolved, but MnC_{60}^+ exohedral formation peaks at 0 eV (no activation barrier), while the activation barrier for MgC_{60}^+ pushes this peak towards higher energies causing the overlap with the high-energy endohedral peak. The low energy edge for the high-energy peak for MgC_{60}^+ is equal to the activation barrier and appears to be in roughly the same spot as for Mn^+. The polynomial fit indicates a threshold near 20 eV for the activation barrier for Mg^+, as compared to approximately 15 eV for Mn^+. This is to be expected, as the same ''window-opening'' [14] insertion mechanism would dominate the process for both Mn^+ and Mg^+ due to their similar sizes.

Having discussed the similarities between the MgC_{60}^+ and MnC_{60}^+ formation processes, there remains the major difference of the activation barrier appearing only for MgC_{60}^+ formation to be explained. The existence of this barrier is chemically reasonable when one considers the relative electron affinities of magnesium and manganese and the concept of the Hard and Soft Acid–Base (HSAB) Principle of Inorganic Chemistry.[15] This concept states that hard acids (low electron affinity acids) will bond easily with hard bases (high electron affinity bases) because the electron will be attracted to the base, forming an ionic bond. While soft acids (high electron affinity acids) bond easily to soft bases (low electron affinity bases) because the electron affinities are similar resulting in shared electrons and thus a covalent bond. It is much less favorable to combine soft acids with hard bases or hard acids with soft bases. Carbon is among the softest of the base atoms, while magnesium is a hard acid, and thus bonding is not very favorable, resulting in the activation barrier to complex formation. Manganese, a much heavier element, is close to the transition between hard and soft acids, thus bonding much more readily with C_{60} resulting in no activation barrier.

Given the statements in the preceding paragraphs, it is necessary and helpful to use optical spectroscopy to provide further evidence for our arguments.

B. Photodissociation of MgC_{60}^+

Although the collision data are interesting in itself, it cannot provide information about the detailed structure of the complexes formed in the collisions. Therefore, laser spectroscopic studies of the complexes were initiated to analyze the structure and stability of these complexes. Although some literature exists providing spectroscopic data on fullerene species in powder, solution, and isolated matrix phases,[1,2,16] the gas phase spectroscopic data presented here contribute to a data set distinguished mainly by its relative paucity.[17] Our studies revealed that the probing radiation had a tendency to dissociate the complexes. Therefore, measurements of both absolute, laser-induced, photodissociation cross-sections and relative branching ratios were carried out with this apparatus. Since the yield of collisional complex generation reactions using the trapping field amplitude modulation technique of the previous section could not provide large enough samples for these measurements, the amplitude modulation was turned off, which resulted in an increase in the Mg^+ density in the trap of several orders of magnitude. The drawbacks are that the kinetic energy of the Mg^+ ions is not well defined due to thermalization with the buffer gas, and the maximum collision energy is limited to less than approximately 20 eV to avoid excessive fragmentation. However the yield in MgC_{60}^+ complexes is greatly enhanced. Two general techniques for observing photodissociation are outlined below, with earlier initial results provided elsewhere.[7,18]

1. Photodissociation branching ratio at 280 nm

There are several possible reaction paths that the photofragmentation of MgC_{60}^+ can follow. These include

$$MgC_{60}^+ + h\nu \rightarrow Mg^+ + C_{60}, \quad \text{(F)}$$

$$MgC_{60}^+ + h\nu \rightarrow Mg + C_{60}^+, \quad \text{(G)}$$

$$MgC_{60}^+ + h\nu \rightarrow C_2 + MgC_{58}^+, \quad \text{(H)}$$

$$MgC_{60}^+ + h\nu \rightarrow MgC_{60}^{2+} + e^-. \quad \text{(I)}$$

Experiments were carried out to test for the presence of each of the above reaction paths. A large number of product ions were generated at collision energies below 15 eV and stored in the ion trap. Photodissociation was carried out by exposure to a strong beam ($\sim$1 mW) of 280 nm laser radiation. To monitor reaction (F), the collected product ions were probed with 280 nm radiation that would cause the Mg^+ ions to fluoresce. Fluorescence was observed, indicating the presence of this reaction channel, but it was difficult to accurately determine the absolute fluorescence yield per reactant ion and thus to determine a quantitative value for this branching ratio. Instead, by process of elimination, this value was determined by measuring all the other branches and assigning the remainder to reaction (F).

The branching ratio for reaction (G) was determined by collisionally generating MgC_{60}^+ and C_{60}^+, and then purging most of the C_{60}^+ out of the trap using secular excitation. A long laser exposure would then be used to dissociate the MgC_{60}^+ and the amount of C_{60}^+ in the trap, produced by photodissociation, would be measured. The experiment was repeated alternating between full laser exposure and no laser exposure (Fig. 7). The ratio between C_{60}^+ counts with full laser exposure and MgC_{60}^+ counts with no laser exposure determined the branching ratio for reaction (G) to be $76 \pm 6\%$ (280 nm laser radiation). In these measurements, care was taken to ensure that the trap was not initially filled with too many ions. When the trap is nearly full (approximately 10^9 ions), effects such as thermal evaporation lead to an appreciable leakage rate out of the trap. However, when ion numbers are kept several orders of magnitude lower, the trap lifetime is measured in hours or longer and thus trap losses will not significantly effect our results.

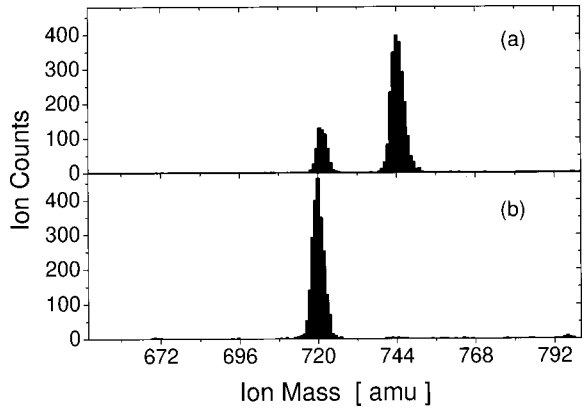

FIG. 7. Typical mass spectra of MgC_{60}^+ and C_{60}^+ ions stored in the trap (a) without any laser irradiation and (b) after exposure to 280 nm laser radiation. In this particular experiment 74% of the photodissociated MgC_{60}^+ apparently fragmented into C_{60}^+.

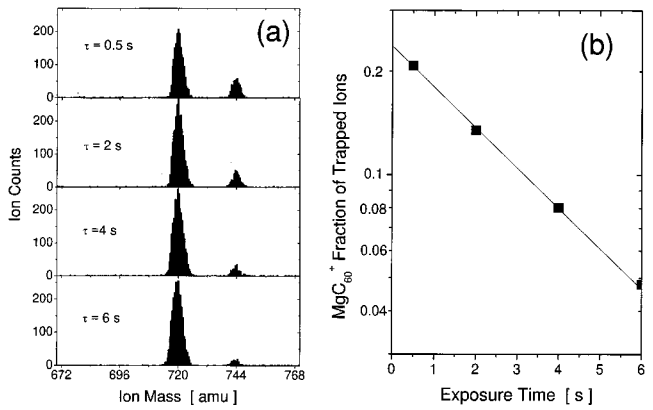

FIG. 8. (a) Mass spectra showing MgC_{60}^+ and C_{60}^+ peaks for four different exposure times (0.5, 2, 4, and 6 s) to 11 mW of 559.9 nm laser radiation. (b) Semilogarithmic plot of the ratio of MgC_{60}^+ ion counts to total ion counts as a function of laser exposure time. The solid line is an exponential fit to the data.

In order to try to detect the presence of fragmented fullerene cages we looked for peaks at masses 696 amu, 672 amu, 648 amu, etc. This is because the MgC_{58}^+ peak and C_{60}^+ peaks are indistinguishable mass spectrometrically. However, given the stability of the C_{60} cage compared to the C_{58} cage as demonstrated in our measurements of fullerene fragmentation by Mg^+ bombardment (Fig. 4), it is reasonable to expect that should C_2 expulsion from MgC_{60}^+ to MgC_{58}^+ occur, then the cascading processes of MgC_{58}^+ to MgC_{56}^+, MgC_{56}^+ to MgC_{54}^+, etc., should also be present resulting in a series of peaks. None of these peaks were observed leading to our conclusion that no significant fragmentation of the fullerene cage [reaction (H)] is occurring at laser powers near 1 mW at 280 nm. Given that our collision data indicates the need for at least 20 eV of collision energy to fragment the fullerene cage, it is reasonable that photon energies below 5 eV (280 nm photons have-about 4.5 eV of energy) are insufficient to break up the cage at relatively low laser intensities where only single photon processes have been observed.[18]

Reaction pathway (I) ionization of the MgC_{60}^+ ion to MgC_{60}^{2+}, could not be seen, and was eliminated from consideration because the 4.5 eV of photon energy is much too low even to overcome the Coulomb attraction energy between an electron and a doubly charged positive ion.

With the above results for reactions (G), (H), and (I), and the fact that we can observe reaction (F) occurring, we assign to reaction (F), the branching ratio of $24\pm6\%$. Table I summarizes these results.

2. Absolute photodissociation cross section of low energy complexes and determination of molecular structures

Building on the results of the previous section, there are two possible techniques for the measurement of the absolute photodissociation cross section of MgC_{60}^+. One can either monitor the destruction of MgC_{60}^+ and the formation of C_{60}^+ mass-spectrometrically, or one can use laser-induced fluorescence to monitor the generation of Mg^+. The former technique involves repeatable loading the trap with identically prepared samples of collisionally generated MgC_{60}^+, and then exposing each sample to a different laser exposure, typically 0.5 s, 2 s, 4 s, and 6 s of a selected laser power and wavelength (Fig. 8). A semilogarithmic plot then yields the photodissociation rate. The latter technique involves a single loading of the trap, but the use of two overlapped laser beams. The pump beam of the selected wavelength and power is used to dissociate the complexes, while a chopped probe beam (5%–10% duty cycle) at 280 nm and very low power (μW) is used to monitor the fluorescence from the trapped sample, and thus the generation of Mg^+ (Fig. 9). The resulting trap fluorescence vs time curves could be fitted to a $(1-e^{-Rt})$ curve to determine the photodissociation rate, after correction for small stray sources of dissociation such as the ultraviolet probe laser beam and trap leakage. Removal of all of the Mg^+ ions from the trap by trap parameter variation is required to ensure an initially zero fluorescence rate

TABLE I. Branching ratio for the photodissociation of MgC_{60}^+, generated at a collision energy of 10 eV, with 280 nm laser radiation at a power density of approximately 3 W/cm^2.

Reaction label	Reaction process	Products	Branching ratio
F	Mg^+ fragmentation	$Mg^+ + C_{60}$	$24\pm6\%$
G	Mg fragmentation	$Mg + C_{60}^+$	$76\pm6\%$
H	Fullerene cage Fragmentation	$C_2 + MgC_{58}^+$	Undetectable
		$C_2 + C_2 + MgC_{56}^+$ etc.	
I	Second ionization	$MgC_{60}^+ + e^-$	n/a

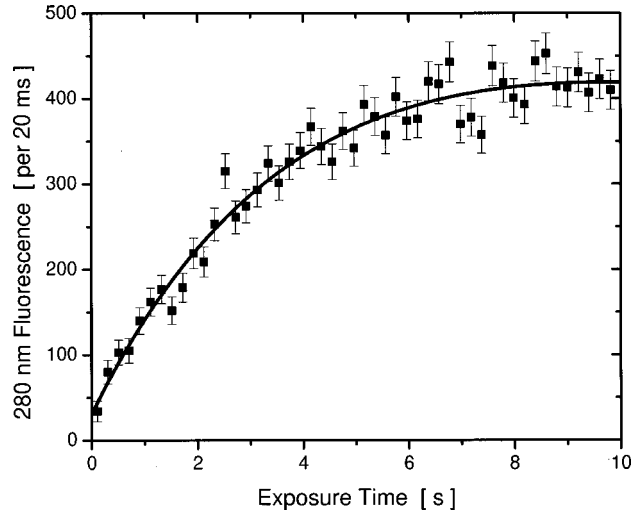

FIG. 9. 280 nm fluorescence intensity as a function of time of exposure to 3.0 mW of 488 nm laser radiation from a trapped sample initially containing no Mg^+ ions. The solid line is an $e^{-\alpha t}(1-e^{-Rt})$. The slow decay in total signal ($e^{-\alpha t}$ factor) appears to result from laser drift rather an actual change in the number of ions.

from the trapped sample. The two techniques provided data that was consistent within experimental error limits. Initial measurements with both of these techniques are described in some detail in Ref. 18.

Measurements of the photodissociation rate as a function of laser intensity yielded linear dependencies, indicating that only single-photon effects were observed at these low laser intensities. This allowed the reaction rate R measured from either technique to be used to calculate the total, absolute, single-photon, photodissociation cross-section via the simple relation,

$$\sigma_{\text{photo}} = 1.6\times 10^{-17} R/P\lambda, \tag{4}$$

where the cross section σ_{photo} is in cm^2, the laser power P is in mW, and the laser wavelength λ is in microns. Equation (4) is derived from a calculation taking into account the partial overlap of the probe laser with the stored ion cloud volume. This results in the dependence on laser power rather than laser intensity (see Refs. 7, 18). The total errors in the cross-sectional values were calculated three ways. First, the uncertainties in the experimental parameters required for these calculations are known (see Table II) and can be propagated through the calculation to generate an overall uncertainty. Second, there is a scatter in the raw data that results in an uncertainty in the fit parameters (fragmentation rate) leading to an uncertainty in the cross section. Finally, two different and independent techniques, mass spectrometry and laser induced fluorescence, can be used to measure the same reaction rate providing a third measure of the uncertainty. All three approaches agreed within an uncertainty in these absolute photodissociation cross sections of $\pm 20\%$.

Using the two techniques, photodissociation cross sections at a number of laser wavelengths and laser powers between 1 and 11 mW were measured in this paper for MgC_{60}^+ and are shown in Fig. 10. A wide range of laser sources was used to carry out these measurements. They are summarized in Table III below. Figure 10 shows the cross section plotted

TABLE II. Calculated uncertainties for the absolute photodissociation cross section of MgC_{60}^+.

Measured quantity ⟨value⟩	Uncertainty in measurement	Effect on absolute cross section
Laser-ion cloud overlap angle	+1°	+7.2%
⟨15°⟩	−1°	−6.4%
Laser beam waist	+100 μm	−7.8%
⟨100 μm⟩	−30 μm	+1.8%
Ion cloud temperature	+100 K	+14.6%
⟨400 K⟩	−100 K	−10.5%
Trap potential	+0.2 eV	+3.9%
⟨2.3 eV⟩	−0.2 eV	−4.5%
Total uncertainty		+16.8%
		−15.2%

vs photon energy. The lowest energy point was measured with a 1300 nm diode laser, and no photodissociation was observed. Based on the experimental noise level, only an upper limit on the rate at this wavelength was possible. Using the nondiode laser data ($\lambda < 650$ nm), a Gaussian curve was fit to the data and is shown in the figure. The diode laser data ($\lambda = 840$ and 1300 nm), taken at a later date, agrees with this initial fit. By integrating the Gaussian curve over photon energy, it is possible to estimate the oscillator strength f of this transition, and thus gain insight into the type of transition, or transitions, which are being observed. An oscillator strength of approximately 0.6 was estimated using this approach, indicating that we are observing a single dipole allowed electronic transition between the ground state and a low number of electronically-excited states. This result greatly simplifies the analysis of this transition process. A reasonable assumption would be that the excited state is a combination of C_{60} and Mg^+ in its first excited state ($1s^2 2s^2 2p^6 3p$), approximately 35 700 cm^{-1} or 4.4 eV above the Mg^+ ground state ($1s^2 2s^2 2p^6 3p$) (see Figs. 11 and 12).

The data provide direct indication of the structure that complexes generated under these conditions actually have. Figures 11 and 12 include a reasonable ground state potential

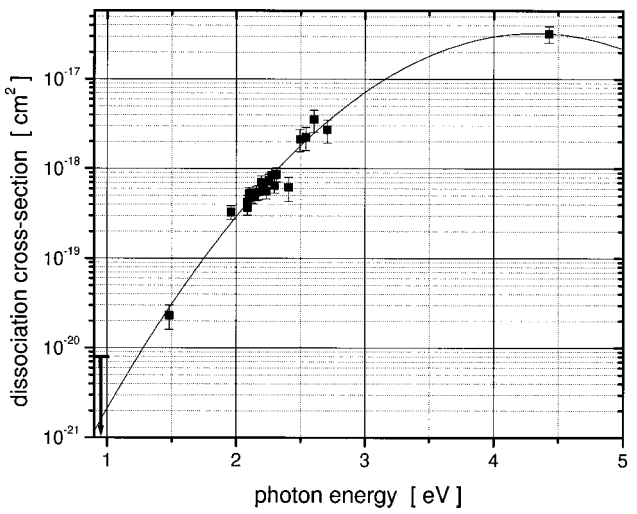

FIG. 10. MgC_{60}^+ absolute, total, photodissociation cross section as a function of probe laser photon energy. The solid line is a Gaussian fit to the data.

TABLE III. Laser sources used for photodissociation measurements.

Laser source type	Output wavelength	Typical laser power
BBO doubling cavity	280 nm	up to 7 mW
Argon ion laser	458, 476, 488, 497, 515 nm	2.5, 3.1, 3.0, 2.6, 7.9 mW
Dye laser	536–594 nm	up to 12 mW
Helium–neon laser	633 nm	4.3 mW
Diode laser	840 and 1300 nm	2 and 5 mW

energy curve for the metallofullerene complex. There is a strong barrier at the radius of the fullerene carbon cage (3.5 Å), thought to be in excess of 10 eV due to the requirement of breaking C–C bonds to insert or remove magnesium ions.[19] A smaller barrier (apparently less than 3 eV) to the formation of exohedral complexes was determined by our collision data and is positioned at a radius in the neighborhood of 5 Å. The potential in the region of the carbon cage radius is produced by the delocalized electron cloud in C_{60} that is approximately 3 Å in thickness. Approximately 2/3 of the cloud is located outside the carbon cage, resulting in a particle-free region of about 2.5 Å in radius at the middle of the fullerene. However, the center of the complex is expected to be not a minimum energy point but a maximum as calculated for other charged guest ions.[20] This results from reduction of energy through interaction of the encapsulated guest ion with the induced dipole moment in the fullerene, or alternately by increased entropy that occurs when the guest ion is moved away from the central, highest symmetry position. This leaves a ground state energy surface with two clear minimums, one for endohedrals and a second for exohedrals. Considering the inner, endohedral, minimum first, the shape of the cross-section, dominated by the Franck–Condon wave function overlap factor, is indicated in Fig. 12. At low photon energies, no break up would occur until the activation barrier is overcome, then there would be a sharp increase in the cross section, followed by a gradual decline as the density of states drops off. The expected ''sharpness'' of the initial increase can be estimated from the Doppler and rotational broadening that can be calculated for the complex. Depending on the position of the Mg nucleus, this broadening should only be between 7 and 112 cm^{-1} (0.5–14 meV).

Comparing this value to the experimental data (Fig. 10), which display a gradual increase over a range in excess of 3 eV, it is clear that these measurements could not be generated by an endohedral complex. However, if one considers the outer exohedral minimum, all that is required is an excited state with no exohedral minimum (see Fig. 12). The upper-state wave function would be concentrated at the turning point and thus would act as a delta-function in the overlap integral resulting in the shape of the photodissociation cross section curve mirroring that of the ground state wave function. Thus the observed Gaussian dependence of the cross section on photon-energy is consistent with these complexes being dominantly exohedral in structure.

The above analysis of our results is based on the assumption that fragmentation occurs via a direct photodissociation process rather than an indirect process such as the molecular analogy to thermionic emission, observed in neutral fullerene photofragmentation reactions by several authors (e.g., Ref. 21). In this process, neutral fullerenes exposed to short pulse, high intensity laser radiation absorb the photons energy and then de-excite via electron emission up to several hundred microseconds after emission. Our apparatus and procedure does not allow us to accurately determine whether the fragmentation is instantaneous or delayed on a microsecond time scale. However, Hansen and Echt showed that the rate of the thermionic process in C_{60} is independent of photon energy over a range of energies (2.3–4.7 eV).[22] Since we observe no plateauing with photon energy of our dissociation cross-section down to values as low as 8×10^{-21} cm^2 it appears reasonable to assume that any indirect contribution to the cross section is less than this amount and thus relatively negligible. It seems physically reasonable that we do not observe these types of thermionic processes

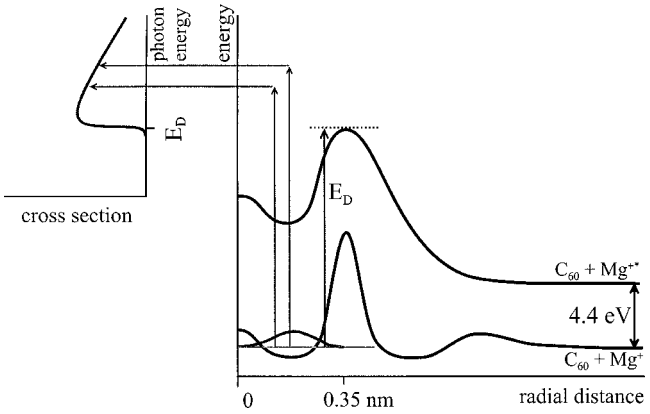

FIG. 11. Potential energy diagram and dissociation cross-section curve for hypothetical photodissociation processes of endohedral MgC_{60}^+ complexes. The Mg^+* indicates the first excited state of Mg^+ (see text).

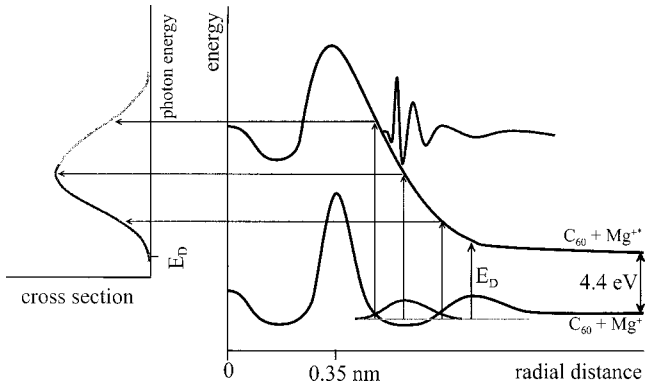

FIG. 12. Potential energy diagram and dissociation cross-section curve for hypothetical photodissociation processes of exohedral MgC_{60}^+ complexes. The Mg^+* indicates the first excited state of Mg^+ (see text).

because of the very low laser intensities (10 mW and below) used in our experiments and the simultaneous viscous cooling of all ions by the buffer gas.

3. Studies of samples containing multiple different species

So far we have discussed optical studies of exohedral complexes. It is even more interesting to be able to generate and identify endohedral complexes. Based on the results of the collision energy resolved data (Sec. III A 3), and on the results of experiments by other groups with different guest atoms [e.g., Mn^+ (Ref. 13)], it is clear that increasing the collision energy will increase the generation of endohedrals. At the same time, too high an energy results in the destruction of all of the fullerene species in the trap. We have observed that destruction increases significantly above approximately 20 eV. Since endohedral generation appears to first appear at energies in this same region, some relatively simple production possibilities do exist. An additional problem is that when an ion is captured by a fullerene, the vast majority of the kinetic energy is converted into internal energy. Basic classical mechanics reveals that when a slow moving massive particle captures a fast moving light particle, the fraction of the light particle's kinetic energy that is converted into internal energy of the new complex is given by the ratio of the large particles initial to final masses. For the case of Mg^+ captured by C_{60} to form MgC_{60}^+, this ratio [mass (C_{60})/mass (MgC_{60})] is 0.968 and thus 97% of the collision energy is converted into rotational and/or vibrational excitation of the complex. Since our experiments study the molecules over long time periods, in the case of the high collision energy needed to generate endohedrals, it is necessary to quickly remove the excess internal energy before the complexes fragment due to excessive vibrational excitation. Therefore, increasing not only the collision energy but also the buffer gas pressure should improve the generation of endohedral complexes. This was subsequently observed when these two quantities were increased, and when the laser exposure time was lengthened. Figure 13 demonstrates the type of data that was observed under these conditions. It shows an initial fast decaying fraction, with a rate matching that from the previous section within experimental uncertainty, followed by a second fraction with a significantly slower decay rate. To study these two fractions, we used the following procedure: The trap was loaded under a suitably chosen set of collisional parameters and then the amount of MgC_{60}^+ present in the trap was measured. The trap would then be reloaded with the same parameters and exposed to between approximately 50 mJ of laser energy, enough to completely destroy the fast decaying fraction but leave a significant portion (approximately $\frac{1}{2}$) of the slow dissociating fraction behind. Day to day variations in the operation of the system required that data for a given experimental plot had to be collected entirely in a single session. Typical results are shown in Figs. 14 and 15. Figure 14 shows this ratio as a function of collision energy for a fixed buffer gas pressure near 3.3 nbar and the filter potential set to 2.5 V. The plot clearly shows the amount of the slow fraction present in the sample dropping to nearly zero as the collision energy was decreased. The

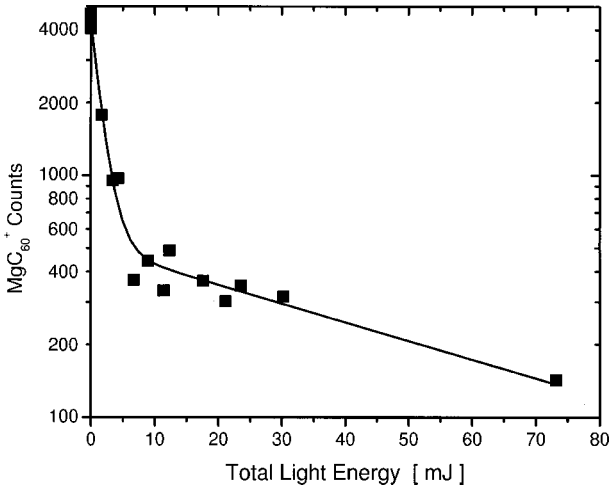

FIG. 13. Semilogarithmic plot showing the amount of MgC_{60}^+ remaining in the trap after various exposures to 280 nm laser radiation. The ordinate is the product of laser power and exposure time, or total laser energy in the exposure. The solid line is a two exponential fit to the data.

gradual tail, rather that a sharp cutoff, can be explained by the fact that the ion source itself was not monoenergetic but has a significant tail in the kinetic energy distribution of the generated ions (see Fig. 16). In most cases, the peak energy ions dominate the reaction and the effect of the higher energy ions in the tail is relatively insignificant. However, when the peak-energy ions cannot react, then the effect of the tail can be seen. Quantitatively, the high energy tail of the Mg^+ source follows an exponential decay of the form e^{-E/E_o}, with the fit shown in Fig. 16 giving a value of $E_o = 2.04 \pm 0.23$ eV for our source. As the collision energy (actually the step potential) is increased, more and more ions in the tail of this distribution have the energy for form the more stable species. Therefore, an offset exponential growth curve with this same constant was then fit to the experimental data as shown by the dotted line in Fig. 14. This excellent match is a strong confirmation of our analysis. The leveling off of

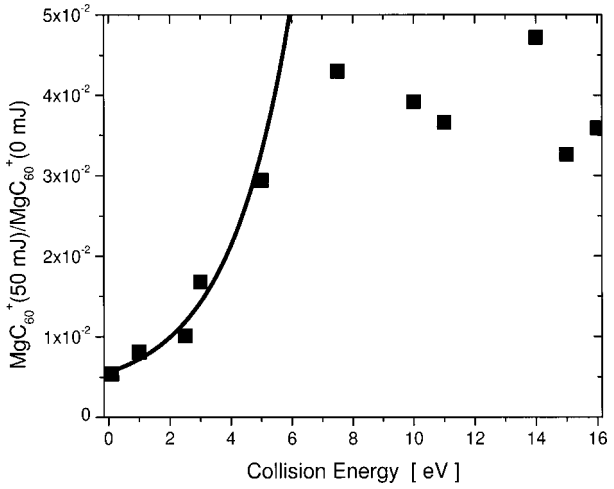

FIG. 14. Plot showing the ratio of the MgC_{60}^+ remaining after exposure to 50 mJ of 280 nm laser radiation to the MgC_{60}^+ in the trap after zero laser exposure, as a function of collision energy. The solid line is an offset exponential growth curve (e^{E/E_o}) with $E_o = 2.05$ eV.

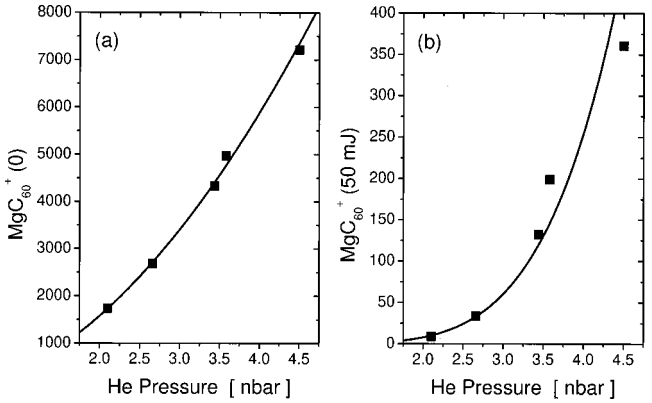

FIG. 15. Plots showing (a) the number of MgC_{60}^+ ions in the trap after zero laser exposure and (b) the number of MgC_{60}^+ remaining after exposure to 50 mJ of 280 nm laser radiation, as a function of helium buffer gas pressure. The solid lines are functional fits to the data of the form (He pressure)^n, with $n=1.9$ in (a) and 5.0 in (b).

the ration above 8 eV mirrors the leveling off of the density of ions produced by the Mg^+ source. Once the lower energy ions are able to form the stable complexes, no further increase in the ratio is possible.

Figure 15 shows the number of ions stored in the trap with and without 50 mJ of 280 nm laser exposure. The collision energy for these measurements is 7 eV. The long-lived fraction size as a function of buffer gas pressure shows that its increase follows a (pressure)^5 curve, roughly three powers more than the pressure dependence of the fast decaying fraction [(pressure)$^{1.9}$]. This is indicative of the need for multiple buffer gas collisions to remove the excess internal energy and stabilize the complex in the case of the slow decaying complexes, which apparently only form in high energy collisions.

These two pieces of data, increased slow-decaying fraction with collision energy and buffer gas pressure, suggest that this fraction requires significantly more energy to form than the slow-decaying exohedral species. Therefore, they both strongly support the hypothesis that the slow decaying fraction has an endohedral structure.

It should be noted that at high collision energies and high buffer gas pressure the size of the slow fraction begins to decrease. In the former case, this is because at high energies fragmentation reactions destroy all fullerene complexes in the trap and both the total number of complexes, and the number of slowly dissociating complexes decreases. In the latter case, this occurs when the trap becomes full, allowing RF heating to preferentially expel those ions formed in higher energy states in the trap's harmonic well. Since endohedral complexes appear to be formed via collisions with the high energy Mg^+ ions, they are created at higher energy states in the well, and thus are subject to stronger RF heating effects than the exohedrals, which were generally formed through collisions with lower energy Mg^+ ions. Therefore, when the trap is near capacity, exohedral complexes, formed at lower energies, are preferentially retained and detected at the end of the experiment.

With optimized conditions, samples with roughly 40% slow fractions could be generated.[23] With step potentials of 10–15 eV, maximum generation of the slow fraction occurred when the buffer gas pressure was set to nearly fill (approximately 80% of capacity) the ion trap. The exact buffer gas pressure depended on the Mg^+ ion and C_{60} molecule densities being utilized. The slow fractions were measured to be at least 20 times slower in fragmentation that the fast samples, although absolute measurements are complicated by sample size and heating effects that appear as the sample size begins to fill the trap.

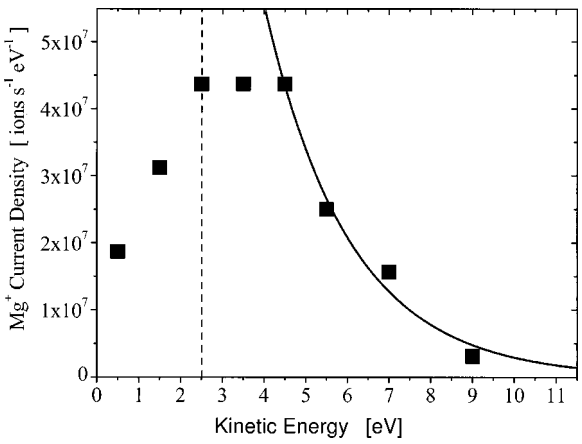

FIG. 16. Kinetic energy distribution of the Mg^+ ion source as determined by varying the filter potential at the injection end of the ion trap. The vertical dashed line at 2.5 eV indicates the ions filtered out of the apparatus to improve the energy resolution of the collision measurements under normal operating conditions. The solid line is an exponential decay fit to the high energy tail of the distribution.

IV. FUTURE DIRECTIONS

Combining these generation parameters with fast laser dissociation of the exohedral complexes and secular filtering of the trap to remove C_{60}^+ ions, the generation of virtually pure, slow-dissociating samples should be possible. With the ability to generate and store what appear to be samples of endohedral MgC_{60}^+ complexes, there is a wide range of possible future experiments. Future steps planned for this work include gas-phase reactivity studies of the slow and fast photodissociating fractions with various reaction partners. These studies should be a useful conformation probing for the position of the Mg atom relative to the fullerene cage. Endohedral complexes would be far less reactive than exohedrals where the highly reactive Mg is exposed to the reactant molecules. Time-resolved mass spectrometry of the ion trap will provide a straightforward method of measuring reaction rates. In addition to acting as a conformation of the fundamental question on the guest particle position, there are many possible reactivity measurements of endohedrals that would be of interest in gas phase chemistry. The gas phase reactivity of fullerenes with several different chemicals is known,[3–5] but no studies of the equivalent fullerene complex reactivities have been carried out so far.

Additional laser photodissociation spectroscopic studies of metallofullerene complexes are also under consideration. The major goal will be to extend the spectroscopic measure-

ments into the much deeper UV to explore regions of interest that are unavailable with CW laser systems. The use of nanosecond pulsed lasers and nonlinear optics opens the possibilities to expose complexes to higher individual photon energies by up to a factor of 3 [90 nm$<\lambda<$270 nm (Ref. 24)].

One other area of interest would be an attempt to observe fluorescence from an encapsulated guest ion in an endohedral complex. The fullerene electron cloud is mainly located outside the carbon cage, leaving a particle free space in the middle. Although the authors know of no published experimental results, there have been theoretical calculations for encapsulated Xe and Ba atoms,[25] as well as alkali metals,[26] which show interesting results. Our experimental data to date, as well as the unknown charge state on an encapsulated Mg-ion suggest that MgC_{60}^+ complexes are not the best candidates for such a study. Other guest ions with higher electron affinities than magnesium, such as rare earth metals, may provide a better system for this kind of investigation.

V. CONCLUSIONS

A series of experiments have been carried out in a linear ion trap with the goal of studying both the formation processes and final molecular structure of collisionally generated MgC_{60}^+ complexes. Both mass spectrometric and laser spectroscopic techniques were utilized for the detection and analysis of these species. Complexes were generated within the trap under controlled collision conditions to study the effect of the collision energy (0–100 eV), ionic density, and buffer gas pressure on the formation process. Laser photodissociation measurements were used to give information on the molecular structure of the collisionally formed species, specifically the location of the Mg^+ guest atom, inside or outside of the carbon cage. Mass spectrometry of the collision products revealed the appearance of fullerene fragment ions above ~25 eV collision energy, while the formation of C_{60}^+ fullerene ions via charge transfer reactions was shown to maximize near 50 eV for Mg^+ collisions. This effect was shown to result from Massey-type resonances in the charge transfer process. The formation of MgC_{60}^+ complexes demonstrated a broad, possibly double peaked structure below 100 eV, with zero formation occurring for collision energies near zero energy. The hypothesis that the possible double peaking results from the production of exohedral complexes at low energies and endohedral complexes at higher energies was further investigated with laser photodissociation spectroscopy. The photodissociation cross-section for complexes formed at low collision energies ($E<15$ eV) was measured to be between 3×10^{-19} and 3×10^{-17} cm^2 for wavelengths in the range 280–656 nm, while infrared photons produced cross sections below 3×10^{-19} cm^{-1}. The energy dependence of the collision process and the form of the dissociation cross-section curve indicate that these measurements were for the exohedral complex MgC_{60}^+. At higher Mg^+ collision energies, a second more slowly dissociating fraction appears. The size of the second fraction increases with increasing collision energy and buffer gas pressure. All of these data support the theory that this second fraction is a highly stable endohedral complex, namely, MgC_{60}^+.

ACKNOWLEDGMENTS

The authors would like to thank Dr. G. Shimuzu of the Department of Chemistry at the University of Calgary for this useful input into the discussion of the HSAB explanation of the fullerene complex formation processes. One of the authors (R.I.T.), would like to acknowledge the support of the Natural Sciences and Engineering Research Council of Canada, while another author (H.A.S.) is grateful to the Applied Research Program of Texas for Advanced Technology Grant No. 010366-082.

[1] K. Kikuchi, S. Suzuki, Y. Nakao, N. Nakahara, T. Wakabayashi, H. Shiromaru, K. Saito, and Y. Achiba, Chem. Phys. Lett. **216**, 67 (1993).
[2] H. Shinohara, M. Inakuma, N. Hayashi, H. Sato, Y. Saito, T. Kato, and S. Bandow, J. Phys. Chem. **98**, 8597 (1994).
[3] S. Petrie, G. Javahery, and D. K. Bohme, Int. J. Mass Spectrom. Ion Processes **124**, 145 (1993).
[4] S. Petrie, G. Javahery, and D. K. Bohme, Astron. Astrophys. **271**, 662 (1993).
[5] S. Petrie, G. Javahery, H. Wincel, Jinru-Wang, and D. K. Bohme, Int. J. Mass Spectrom. Ion Processes **138**, 187 (1994).
[6] E. E. B. Campbell *et al.*, Phys. Rev. Lett. **84**, 2128 (2000).
[7] M. Welling, H. A. Schuessler, R. I. Thompson, and H. Walther, Int. J. Mass Spectrom. Ion Processes **172**, 95 (1998).
[8] P. Scheier, B. Dunser, R. Worgotter, D. Mugg, S. Matt, O. Echt, M. Foltin, and T. D. Mark, Phys. Rev. Lett. **77**, 2654 (1996).
[9] R. E. Johnson, *Introduction to Atomic and Molecular Collisions* (Plenum, New York, 1982), p. 136.
[10] C. E. Moore, *Atomic Energy Levels, Vol. 1, Circular of the National Bureau of Standards 467* (United States Department of Commerce, Washington, D.C., 1949), p. 106.
[11] R. K. Yoo, B. Ruscic, and J. Berkowicz, J. Chem. Phys. **96**, 911 (1992).
[12] Z. Wan, J. F. Christian, and S. L. Anderson, J. Chem. Phys. **96**, 3344 (1992).
[13] Y. Basir and S. L. Anderson, Chem. Phys. Lett. **243**, 45 (1995).
[14] M. Saunders, R. J. Cross, H. A. Jiminez-Vazquez, R. Shimshi, and A. Khong, Science **271**, 1693 (1996).
[15] G. Wulfsberg, *Principles of Descriptive Inorganic Chemistry* (University Science Books, Sausalito, CA, 1991), p. 266.
[16] A. Sassara, G. Zerza, and M. Chergui, J. Phys. B **29**, 4997 (1996).
[17] A. L. Smith, J. Phys. B **29**, 4975 (1996).
[18] M. Welling, R. I. Thompson, and H. Walther, Chem. Phys. Lett. **253**, 37 (1996).
[19] E. E. B. Campbell, R. Ehlrich, G. Heusler, O. Knospe, and H. Sprang, Chem. Phys. **239**, 299 (1998).
[20] J. L. Ballester and B. I. Dunlap, Phys. Rev. A **45**, 7985 (1992).
[21] C. E. Klots and R. N. Compton, Surf. Sci. Lett. **3**, 535 (1996).
[22] K. Hausen and O. Echt, Phys. Rev. Lett. **78**, 2337 (1997).
[23] R. I. Thompson, M. Welling, and H. Walther, *Recent Advances in the Chemistry and Physics of Fullerenes: Volume 4*, edited by K. M. Kadish and R. S. Ruoff (The Electrochemical Society Proceedings Series, PV 97-14, Pennington, 1997), pp. 70–81.
[24] J. G. Eden, Can. J. Phys. **78**, 397 (2000).
[25] M. J. Puska and R. M. Nieminen, Phys. Rev. A **47**, 1181 (1993).
[26] M. S. Dresselhaus, G. Dresselhaus, and P. C. Eklund, *Science of Fullerenes and Nanotubes* (Academic, San Diego, CA,1996), p. 224.